

Measurement and calculation of the orientation dependence of terahertz pulse detection in ZnTe

Paul C. M. Planken

*Department of Applied Physics, Faculty of Applied Sciences, Delft University of Technology,
Lorentzweg 1, 2628 CJ Delft, The Netherlands*

Han-Kwang Nienhuys and Huib J. Bakker

FOM Institute for Atomic and Molecular Physics, Kruislaan 407, 1098 SJ Amsterdam, The Netherlands

Tom Wenckebach

*Department of Applied Physics, Faculty of Applied Sciences, Delft University of Technology,
Lorentzweg 1, 2628 CJ Delft, The Netherlands*

Received June 28, 2000; revised manuscript received October 23, 2000

We have performed measurements and calculations of the efficiency of terahertz (THz) detection in ZnTe as functions of the angle between the THz polarization and the crystal (001) axis of the angle between the THz polarization and the probe-beam polarization. We find that, for angles of 0° and 90° between the probe and THz polarization, the THz detection process is most efficient, whereas the commonly used angle of 45° gives less than optimal results. In addition, we show how the polarization direction of a THz beam can be found if the direction of the crystal (001) axis is known. Our results are valid for ZnTe and other zinc-blende crystals such as GaP. © 2001 Optical Society of America

OCIS codes: 300.6270, 190.7110, 320.7130, 190.2620.

1. INTRODUCTION

The generation and detection of subpicosecond single-cycle electromagnetic transients with femtosecond laser pulses is gaining widespread acceptance as a convenient method of gaining access to the terahertz (THz) frequency range. THz pulses are now used for linear spectroscopy,^{1–3} ranging,⁴ and two-dimensional imaging.^{5,6} As far as the detection of THz pulses is concerned, roughly three types of device have been described in the literature: bolometers,^{7,8} time-gated antennas,³ and time-gated electro-optic detectors.^{9–12} The advantage of time-gated detection over bolometric detection is the inherent suppression of the thermal background.

Electro-optic detection is a second-order nonlinear optical process in which an applied electric field induces a refractive-index change in an electro-optic material at visible–near-IR frequencies that is proportional to the applied field. This refractive-index change affects the ellipticity of a circularly polarized, synchronized, ultrashort laser pulse that is copropagating through the same material. This change in ellipticity is measured with a polarizing beam splitter that separates the two orthogonal polarization components of the probe beam. A balanced photodetector measures the intensity difference between the two components and gives a signal that is directly proportional to the electric field. By varying the delay between the THz pulse and the probe-laser pulse, one obtains the complete time-dependent electric field. Electro-optic detection is emerging as the most popular choice for

THz detection. There are two reasons for this: First, electro-optic materials are readily commercially available, unlike time-gated antennas, which typically require that one use microfabrication techniques to make them. Second, electro-optic detection is suitable for signals with a large bandwidth (70 THz has been demonstrated¹³), much larger than the 3-dB bandwidth of antennas of 1 THz. Because of the numerous applications of THz pulses, obtaining a good signal-to-noise ratio in the electro-optic detection of a THz electric field is essential. Improving the signal detection allows one to reduce the measurement time. For electro-optic detection, zinc-blende crystals such as ZnTe and GaP are often used. Of these, ZnTe is very suitable because its refractive index in the far IR is comparable to the near-IR refractive index, resulting in relatively efficient THz detection. It is therefore surprising that, to our knowledge, no detailed study has been published that describes the optimal configuration for electro-optic detection in ZnTe. As we show below, finding the optimal configuration experimentally is not a trivial exercise because of the many degrees of freedom, such as the probe-beam polarization direction and the THz polarization direction with respect to the crystal (001) axis, in the detection system. In this paper we therefore present measurements and calculations of THz pulse detection in (110)-oriented ZnTe, showing the THz detection efficiency as a function of the angles of the probe-beam polarization and the THz polarization with respect to the crystal (001) axis.

2. EXPERIMENTAL SETUP

The experimental setup for generating THz pulses uses a 1-kHz repetition-rate, amplified Ti:sapphire laser capable of generating 100-fs pulses with energy of 3 mJ. The laser beam is split in two. A small fraction ($\ll 1\%$) is used as a probe pulse. The largest fraction of the beam passes through an optical delay line that is scanned at a 1-Hz repetition rate. The pump beam is then expanded to a diameter of 2.5 cm by use of a telescope and directed toward a (100)-oriented GaAs wafer, which is at an angle of 45° with respect to the beam. The beam illuminates a region on the GaAs wafer between two parallel electrodes that are spaced 3.5 cm apart and biased with voltage pulses with a peak amplitude of up to 20 kV and a duration of $30 \mu\text{s}$. The repetition rate of the voltage source is 500 Hz, so every odd-numbered laser pulse coincides with a voltage pulse on the wafer. When the wafer is biased, a THz pulse is emitted from the wafer in the direction of the reflected laser pulse, with a polarization determined by the direction of the applied electric field. The remainder of the setup is shown in Fig. 1(a). With parabolic mirrors, the generated THz pulses are focused onto a 0.5-mm-thick (110)-oriented ZnTe crystal, which is mounted

on a rotation stage. The probe pulse passes through a half-wave plate and a polarizer, allowing us to rotate its polarization. Figure 1(b) shows the directions and polarizations of the probe and THz beams in the ZnTe crystal. The probe pulse is focused onto the same spot on the ZnTe crystal as the THz beam. After the crystal, the probe beam passes first through a quarter-wave plate and then through a Wollaston prism, which separates the two orthogonal polarization components. A differential detector measures the different intensities of the two polarization components. When the delay is scanned at a 1-Hz frequency, a THz temporal scan, corresponding to a 15-ps delay, is obtained, with a signal-to-noise ratio of 30. Although it might seem strange to use a rapid scan technique for a laser with a repetition rate of only 1 kHz, this technique actually offers an important advantage over conventional slow-scan methods: As the laser noise is dominated by power fluctuation on a time-scale longer than 1 s, the rapid scan technique suppresses noise with a frequency of less than 1 Hz. This improves the overall signal-to-noise ratio with which we detect the THz electric field.

3. RESULTS

An example of a measured THz electric field as a function of delay, averaged over a thousand scans, is shown in Fig. 2. The electric field is a quasi-half-cycle pulse typical for biased GaAs THz emitters^{7,14,15} and has a signal-to-noise ratio of approximately 10^3 . At a time delay of approximately 10 ps, the signal increases again, corresponding to a reflection of the THz electric field in the ZnTe crystal. The oscillations from 1 to 9 ps are caused by the absorption and subsequent emission of light by water-vapor molecules. We define α as the angle of the THz beam polarization with respect to the (001) axis and φ as the angle of the probe-beam polarization with respect to the crystal (001) axis. Figure 3 shows the measured maxima of the THz amplitude as a function of the crystal's azimuthal angle α when the probe-beam polarization is perpendicular to the THz polarization. These maxima are obtained from electric field temporal scans such as the one shown in Fig. 2 but averaged over only 10 scans, resulting in a signal-to-noise ratio of approximately 100. Ignoring the sign of the amplitude, we note that when the crystal is rotated around the (110) axis the detected THz signal shows two absolute maxima when $\alpha = 90^\circ$ and $\alpha = 270^\circ$ and four minor amplitude maxima at angles in between. Measurements for angles between the THz polarization and the probe-beam polarization of 45° and 0° are also shown in Fig. 3. Note that, as the probe-beam polarization is changed, both the orientation of the quarter-wave plate and the Wollaston prism have to be adjusted. When $\varphi = \alpha + 45^\circ$, we observe four major absolute maxima and two minor maxima. The curve for $\varphi = \alpha$ is identical to the curve for $\varphi = \alpha + 90^\circ$ when we multiply the former by a factor of -1 . Interestingly, a comparison of the maximum signals obtained for the three different angles between the THz polarization and the probe-beam polarization shows that the maximum signal is obtained not for the commonly chosen angle of $\varphi = \alpha + 45^\circ$ but for $\varphi = \alpha + 90^\circ$ or $\varphi = \alpha$. We thus obtain small but mea-

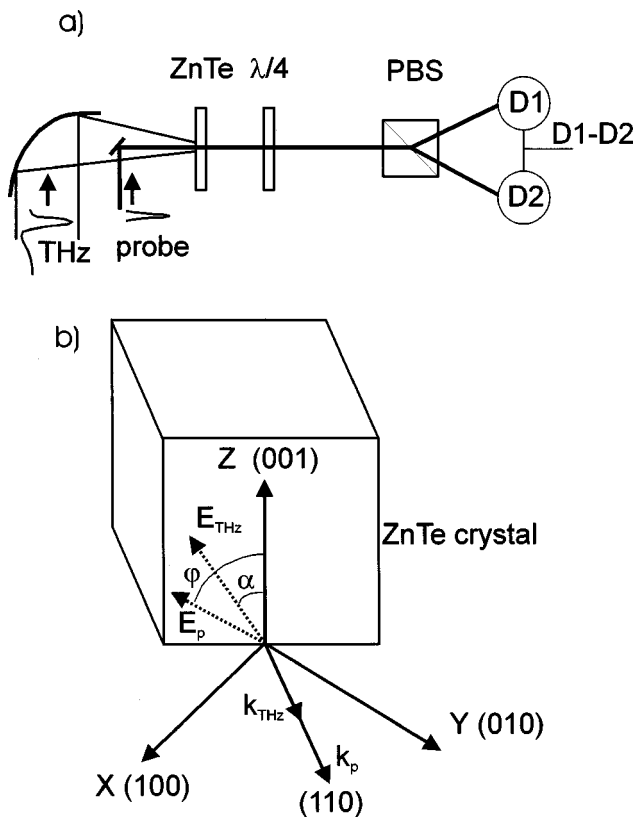


Fig. 1. (a) Experimental setup for detection of the electric field of THz pulses. Both the THz beam and the probe beam are focused on a ZnTe crystal. After the crystal, the probe beam passes through a quarter-wave plate and a polarizing beam splitter (PBS). A differential detector (consisting of photodiodes D1 and D2) measures the difference D1–D2, which is proportional to the THz electric field. (b) Angles of the THz and probe-beam polarization directions with respect to the crystal z axis. k_{THz} and k_p give the propagation directions of the THz and the probe beam, respectively. x corresponds to the (100) axis, y to the (010) axis, and z to the (001) axis.

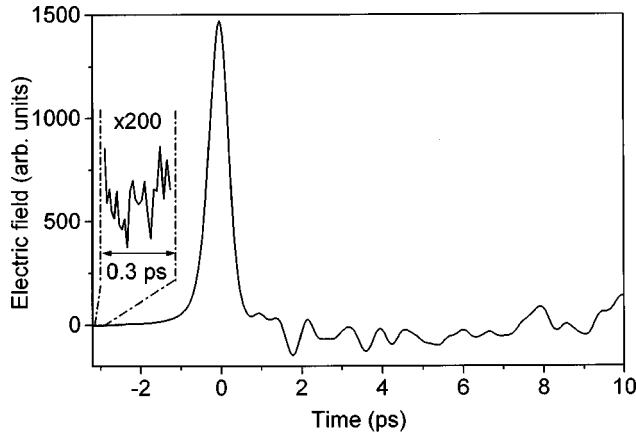


Fig. 2. Measured THz electric field generated by illumination of the area between biased electrodes on a GaAs wafer. The measurement is a 17-min average over 1000 temporal scans. A blowup of the first 0.3 ps (inset) shows that the signal-to-noise ratio obtained in this measurement is approximately 1000.

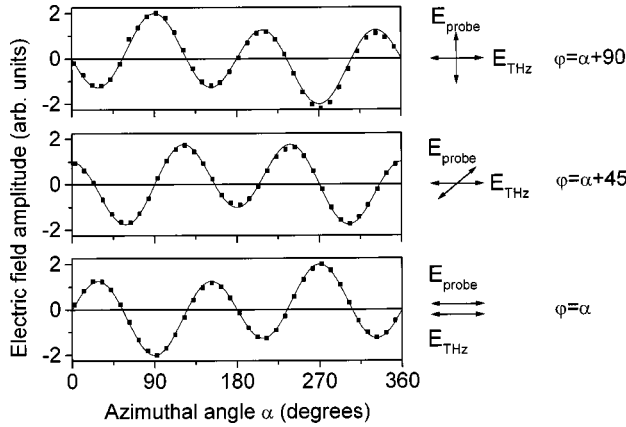


Fig. 3. Measured dependence on the crystal's azimuthal angle α of the detected THz electric field for three different fixed angles between the probe-beam polarization and the THz polarization.

surable improvement in the signal-to-noise ratio by choosing the correct polarization angles. In Section 4 a theoretical description is presented that correctly predicts the measured orientation dependence of THz detection.

4. ANALYSIS AND DISCUSSION

The starting point for our calculation of the THz detection efficiency is the refractive-index ellipsoid that arises when an electric field is applied to the crystal. This index ellipsoid defines the refractive index in the crystal that is experienced by, for example, visible-near-IR light propagating through the crystal with a given propagation direction and polarization. For a cubic crystal such as ZnTe, with point group $\bar{4}3m$, the only nonzero coefficient of the electro-optic tensor is r_{41} .¹⁶ If x , y , and z define the coordinate axes in the crystal, with the z axis corresponding to the (001) crystal axis, the refractive-index ellipsoid is given by

$$x^2/n^2 + y^2/n^2 + z^2/n^2 + 2E_{\text{THz},1}r_{41}yz + 2E_{\text{THz},2}r_{41}xz + 2E_{\text{THz},3}r_{41}xy = 1, \quad (1)$$

where $E_{\text{THz},1}$, $E_{\text{THz},2}$, and $E_{\text{THz},3}$ are the components of the applied THz field \mathbf{E}_{THz} along the x , y , and z directions, respectively, and where n is the unperturbed refractive index. The presence of the mixed terms yz , xz , and xy in Eq. (1) indicates that the main axes of the ellipsoid do not coincide with the coordinate axes. The main problem is to find a coordinate transformation such that the main axes of the ellipsoid are aligned with the new coordinate axes. Then, by projecting the probe-laser polarization on these axes, we can calculate the effect that the field-induced refractive-index change has on the pulse polarization as it propagates through the crystal. We can make an immediate simplification by noting that, for a THz pulse propagating along the (110) axis, $E_{\text{THz},2} = -E_{\text{THz},1}$. After studying Eq. (1), we find that we need two coordinate transformations to align the index ellipsoid with the new coordinate axes. The first transformation is a rotation of 45° around the z axis,

$$\begin{aligned} x &= \frac{1}{2}\sqrt{2}x' - \frac{1}{2}\sqrt{2}y', \\ y &= \frac{1}{2}\sqrt{2}x' + \frac{1}{2}\sqrt{2}y', \\ z &= z'. \end{aligned} \quad (2)$$

Equations (2) transform the ellipsoid into the form

$$\begin{aligned} x'^2 \left(\frac{1}{n^2} + E_{\text{THz},3}r_{41} \right) + y'^2 \left(\frac{1}{n^2} - E_{\text{THz},3}r_{41} \right) + \frac{z'^2}{n^2} \\ + 2\sqrt{2}E_{\text{THz},1}r_{41}y'z' = 1. \end{aligned} \quad (3)$$

From the remaining mixed $y'z'$ term in Eq. (3) we deduce that a final rotation of the (x', y', z') system around the x' axis is needed to align the coordinate system with the main axes of the index ellipsoid. Taking the angle over which the coordinate system is rotated to be θ , we can write for the transformation

$$\begin{aligned} x' &= x'', \\ y' &= y'' \cos \theta - z'' \sin \theta, \\ z' &= y'' \sin \theta + z'' \cos \theta. \end{aligned} \quad (4)$$

We express the components of the electric field in terms of the angle α : $E_{\text{THz},3} = E_{\text{THz}} \cos \alpha$ and $E_{\text{THz},1} = E_{\text{THz}}/2\sqrt{2} \sin \alpha$, with $E_{\text{THz}} = |\mathbf{E}_{\text{THz}}|$. With these definitions and after some calculus, we find for the index ellipsoid

$$\begin{aligned} x''^2 \left(\frac{1}{n^2} + E_{\text{THz}}r_{41} \cos \alpha \right) \\ + y''^2 \left\{ \frac{1}{n^2} - E_{\text{THz}}r_{41} [\cos \alpha \sin^2 \theta + \cos(\alpha + 2\theta)] \right\} \\ + z''^2 \left\{ \frac{1}{n^2} - E_{\text{THz}}r_{41} [\cos \alpha \cos^2 \theta - \cos(\alpha + 2\theta)] \right\} \\ = 1, \end{aligned} \quad (5)$$

provided that

$$2\theta = -\arctan(2 \tan \alpha) - n\pi,$$

$$\left(n - \frac{1}{2}\right)\pi \leq \alpha < \left(n + \frac{1}{2}\right)\pi, \quad n = 0, 1, \dots \quad (6)$$

The angle θ over which we rotate the coordinate system around the x' axis is thus a function of the angle α between the THz polarization and the (001) axis. For small electric fields, we obtain from Eq. (5) the refractive indices for visible–near-IR light propagating along the x'' direction

$$n_{y''}(\alpha) \approx n + \frac{n^3}{2} E_{\text{THz}} r_{41} [\cos \alpha \sin^2 \theta + \cos(\alpha + 2\theta)],$$

$$n_{z''}(\alpha) \approx n + \frac{n^3}{2} E_{\text{THz}} r_{41} [\cos \alpha \cos^2 \theta - \cos(\alpha + 2\theta)], \quad (7)$$

where θ is given by Eq. (6). From relation (7) it is clear that $n_{y''}$ and $n_{z''}$ are different and therefore that the electric field polarization components of the probe-laser field, E_p , in the y'' and z'' directions accumulate different optical phases. As a result, the probe field becomes elliptically polarized. The intensity difference, ΔI , of the polarization components that correspond to the ellipse can easily be calculated:

$$\Delta I(\alpha, \varphi) = I_p \sin[2(\varphi - \theta)] \sin\left\{\frac{\omega}{c}[n_{y''}(\alpha) - n_{z''}(\alpha)]L\right\}, \quad (8)$$

where L is the crystal length, I_p is the probe intensity, c is the velocity of light in vacuum, and ω is the angular frequency of the probe pulse. When the field-induced phase difference is small, we can replace the second sine in Eq. (8) with its argument. Using Eq. (6) and relation (7), we can then simplify the equation to

$$\Delta I(\alpha, \varphi) = I_p \frac{\omega n^3 E_{\text{THz}} r_{41} L}{2c} (\cos \alpha \sin 2\varphi + 2 \sin \alpha \cos 2\varphi). \quad (9)$$

Equation (9) shows that the signal from the balanced detector is proportional to the applied electric field. This equation also demonstrates that a purely experimental determination of the maximum signal is difficult. This is so because we have to vary both the polarization direction of the THz pulse and the polarization direction of the probe-laser pulse independently to find the maximum signal. However, an analysis of Eq. (9) shows that the maximum signal $\Delta I(\alpha, \varphi)$ can be obtained when $\varphi = \alpha + 90^\circ$ or $\varphi = \alpha$. In Fig. 3 we plot the results of the calculations of the orientation dependence of THz detection in ZnTe for the three different angles used in the experiment. The calculations are based on Eq. (9) and are in excellent agreement with the measurements, showing the correct maxima and minima in the THz detection efficiency as a function of the azimuthal angle. The results clearly demonstrate how the detected THz signal is a function of the orientation of the THz polarization with respect to the crystal (001) axis and of the orientation of

the THz polarization with respect to the probe-beam polarization. Equations (8) and (9) are therefore quite important for the experimentalist wishing to optimize the THz detection efficiency.

It should be noted that Eqs. (8) and (9) are valid for all THz frequencies. The frequency dependence of the values of the near-IR refractive-index n (2.8 for ZnTe at 800 nm) and the electro-optic coefficient r_{41} (3.9 pm/V for ZnTe at $\omega_{\text{THz}} = 0$;) determines the shape and amplitude of the THz waveform but not the shapes of the curves of the orientation dependence of the THz detection efficiency. The frequency dependences of the refractive index and the electro-optic coefficient are not functions of the crystal's azimuthal angle.

Without having to resort to wire-grid polarizers, we can also use Eq. (9) to find the polarization direction of a linearly polarized THz beam, provided that the direction of the (001) axis of the (110)-oriented crystal is known. Keeping $\varphi = 0$ while we rotate the crystal around the (110) axis, we can see from Eq. (9) that the intensity difference becomes zero when $\alpha = 0$. In other words, when the intensity difference is zero, the THz polarization is parallel to the (001) axis of the crystal. The presence of elliptically polarized light can be inferred from the fact that for $\varphi = 0$ there is no angle α for which the intensity difference disappears. Finally, we note that, although we performed the experiments with ZnTe, the theoretical expressions derived are equally valid for the other zincblende crystals, such as GaP.

5. CONCLUSIONS

We have performed measurements and calculations that show how the efficiency of THz detection strongly depends on the orientation of the THz polarization with respect to the crystal (001) axis and on the angle between the probe-beam polarization and the THz polarization. We find that the optimum angles between the THz and the probe-beam polarizations are 0° or 90° . In addition, we describe a simple procedure to determine the polarization direction of a linearly polarized THz beam, based on the assumption that the (001) axis of the (110)-oriented ZnTe (or GaP) is known.

ACKNOWLEDGMENT

We thank R. N. Schouten for expert electronics support. P. C. M. Planken's e-mail address is planken@hwork3.tn.tudelft.nl.

REFERENCES

1. D. Grischkowsky, S. Keiding, M. van Exter, and Ch. Fattinger, "Far-infrared time-domain spectroscopy with terahertz beams of dielectrics and semiconductors," *J. Opt. Soc. Am. B* **7**, 2006–2015 (1990).
2. T.-I. Jeon and D. R. Grischkowsky, "Observation of a Cole-Davidson type complex conductivity in the limit of very low carrier densities in doped silicon," *Appl. Phys. Lett.* **72**, 2259–2261 (1998).
3. M. van Exter and D. R. Grischkowsky, "Characterization of an optoelectronic terahertz beam system," *IEEE Trans. Microwave Theory Tech.* **38**, 1684–1691 (1990).

4. R. A. Cheville and D. Grischkowsky, "Time-domain terahertz impulse ranging studies," *Appl. Phys. Lett.* **67**, 1960–1962 (1995).
5. D.-M. Mittleman, R. H. Jacobsen, and M. C. Nuss, "T-ray imaging," *IEEE J. Sel. Top. Quantum Electron.* **2**, 679–692 (1996).
6. S. Hunsche, M. Koch, I. Brener, and M. C. Nuss, "THz near-field imaging," *Opt. Commun.* **150**, 22–26 (1998).
7. D. You, R. R. Jones, P. H. Bucksbaum, and D. R. Dykaar, "Generation of high-power sub-single-cycle 500-fs electromagnetic pulses," *Opt. Lett.* **18**, 290–292 (1993).
8. M. Joffre, A. Bonvalet, A. Migus, and J.-L. Martin, "Femtosecond diffracting Fourier-transform infrared interferometer," *Opt. Lett.* **21**, 964–966 (1996).
9. Q. Wu and X.-C. Zhang, "Ultrafast electro-optic field sensors," *Appl. Phys. Lett.* **68**, 1604–1606 (1996).
10. Q. Wu, M. Litz, and X.-C. Zhang, "Broadband detection capability of ZnTe electro-optic field detectors," *Appl. Phys. Lett.* **68**, 2924–2926 (1996).
11. Q. Wu and X.-C. Zhang, "7 terahertz broadband GaP electro-optic sensor," *Appl. Phys. Lett.* **70**, 1784–1786 (1997).
12. P. Uhd Jepsen, C. Winnewisser, M. Schall, V. Schyja, S. R. Keiding, and H. Helm, "Detection of THz pulses by phase retardation in lithium tantalate," *Phys. Rev. E* **53**, R3052–3054 (1996).
13. A. Leitensdorfer, S. Hunsche, J. Shah, M. C. Nuss, and W. H. Knox, "Femtosecond charge transport in polar semiconductors," *Phys. Rev. Lett.* **82**, 5140–5143 (1999).
14. D. You and P. H. Bucksbaum, "Propagation of half-cycle far-infrared pulses," *J. Opt. Soc. Am. B* **14**, 1651–1655 (1997).
15. S.-G. Park, A. M. Weiner, M. R. Melloch, C. W. Siders, J. L. W. Siders, and A. J. Taylor, "High-power narrow-band terahertz generation using large-aperture photoconductors," *IEEE J. Quantum Electron.* **35**, 1257–1267 (1999).
16. A. Yariv, *Quantum Electronics*, 2nd ed. (Wiley, New York, 1975).